Leibniz-Gemeinschaft

Final report

# Title of the project:

High average power ultrashort laser pulses in the near and mid-infrared by chirped optical parametric amplification

Leibniz-Institute: Max Born Institute
Reference number: SAW-2012-MBI-2
Project period: 06.01.2012-31.05.2016
Contact partner: Dr. Mark Merö

# Executive Summary

The study of molecular reaction dynamics and structural transformations of molecules through coincident photo-fragment ion imaging, time-resolved photoelectron holography, and laser-induced electron diffraction can tremendously benefit from the development of high repetition rate (i.e. >> 10 kHz) few-cycle optical driver pulses at wavelengths significantly beyond the limit of Ti:sapphire oscillator-amplifier systems (i.e. >> 1 μm). Optical parametric chirped pulse amplification (OPCPA) combined with diode-pumped, picosecond, Yb-laser amplifier pump sources near 1 μm is an average-power-scalable approach for generating the required driver pulses for the above applications. Based on this approach, the main objective of the project was the development of a dual beamline few-cycle OPCPA system providing optically synchronized pulses at 1.5 and 3 μm at an average power beyond the level of contemporary state of the art sources at a repetition rate of about 100 kHz. The target, several 10-μJ pulse energies at 1.5 and 3 μm were to be achieved, on the basis of the availability of unique pump pulse parameters that push the existing technological limits, and that also allow further extension of the OPCPA system for widening its applicability. Another major objective was active carrier envelope phase (CEP) stabilization of the 1.5-μm beamline originating from a yet to be acquired commercial turn-key Er-fiber laser seeder. As the characteristics of the Er-fiber laser were unknown and the proposed "feed-forward" CEP stabilization technique had never been applied before to lasers other than Ti:sapphire oscillators, this proposal was considered as one of the main project risks. Finally, to demonstrate the capabilities of the unique source, application experiments on strong field laser-molecule interactions and imaging were planned.

In accordance with the proposal, we developed a dual-beam OPCPA system providing few-cycle pulses at 1.55 and 3.1 μm with an unprecedented combination of wavelengths, average power, pulse energy, and pulse duration, where only a small fraction of the total available pump power was utilized. In contrast to similar existing systems, our system is based on a more robust nonlinear crystal in the booster amplifier stage, enabling higher conversion efficiency with fewer stages. In spite of inventing a modified version of the feed-forward CEP stabilization scheme allowing an order-of-amplitude increase in servo bandwidth, active CEP stabilization at 1.5 μm was prevented by the extreme noise of the available seeder laser. The capabilities of the OPCPA were demonstrated by a series of experiments on strong-field Coulomb explosion of $CO_2$, water, and acetone. Benefitting from the high repetition rate of the OPCPA, fragment ions resulting from multi-electron ionization could be detected in coincidence. These experiments demonstrated the ability of the OPCPA system to be used in long-term application experiments. Furthermore, proof-of-concept experiments on the applications foreseen for the OPCPA were successfully carried out using available, lower repetition rate laser systems.

From the point that presently has been reached, further scaling of the average power is straightforward using the remaining pump power. This will lead to hitherto inaccessible average powers and peak intensities paving the way for imaging molecular structures and chemical reactivity with attosecond time and picometer spatial resolution.

Table of Contents

# Contents



The basic layout of the optical driver source follows that described in detail in the proposal. First, the implementation of the three work packages (WPs) associated with the three main components of the OPCPA system will be discussed. Then, the fourth WP concerning the implementation of the application experiments will follow.

**WP1: seed source for OPCPA and pump laser**

As the front-end seed laser, a commercial, multi-branch Er-fiber laser system was planned to provide optically synchronized pulses both for the 1.0-µm pump and for the 1.5-µm signal beam of the OPCPA.

**WP1.1: characterization of the fiber laser seed source**

Initial questions:

- pulse duration, chirp, and spectrum near 1.5 µm,
- pulse energy at 1.5 and 1.0 µm,
- relative timing jitter between the 1.5-µm and 1.0-µm pulses,
- long term stability of energy, spectral phase at 1.5 µm and energy at 1.0 µm.

Actual implementation:

A three-branch commercial Er-fiber laser system was acquired. The three branches correspond to three modules. The master module contains an 80-MHz oscillator, an amplifier, a prism compressor, and a highly nonlinear fiber (HNLF). The two slave modules are supercontinuum modules, which are seeded from the master module and contain only amplifiers, prism compressors, and HNLF's. The first supercontinuum module is used in combination with a commercial f-2f interferometer, while the second one provides the seed pulses for the pump amplifier chain. The pulses were characterized using a home-built second-harmonic generation (SHG) FROG device. Accordingly, it was determined that sub-30-fs, nearly transform limited pulses were provided from the master module with an unexpected, several-100-fs long pedestal and a highly structured spectrum centered at 1.56 µm (cf. Fig. 1 and 2). The pulse energy at 1.56 µm is sufficiently large (i.e. 3.5 nJ at 80 MHz) to accommodate the losses due to CEP correction. The spectral energy density near 1.0 µm, however, is only 2 pJ/nm and does not provide much headroom for losses before amplification. The relative timing jitter between the different branches was considered negligible compared to the timing jitter expected directly at the OPCPA stages, which could be characterized only after the implementation of the complete pump amplifier chain. The long term stability was found to be limited by the stability of the ambient temperature, as the modules were not thermally stabilized. Furthermore, a warm-up time of > 4 hours was needed to reach a stable spectral phase and supercontinuum spectrum. Once the initial > 4-hour warm-up time is reached and the lab temperature is stable within ±0.2 $^{o}$C, the modules operate in a stable manner without the need of any adjustment for weeks.

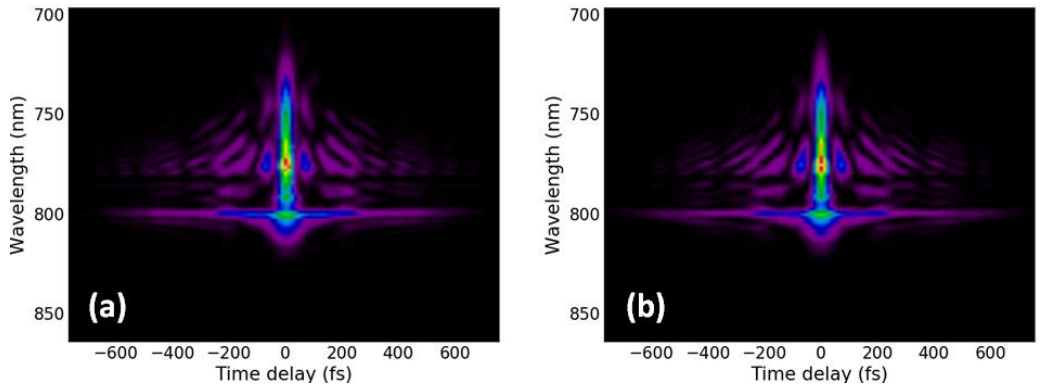


**Fig. 1** (a) measured SHG-FROG trace, (b) retrieved SHG-FROG trace for the 1.56-µm OPCPA seed pulses at the output of the Er-fiber laser module.

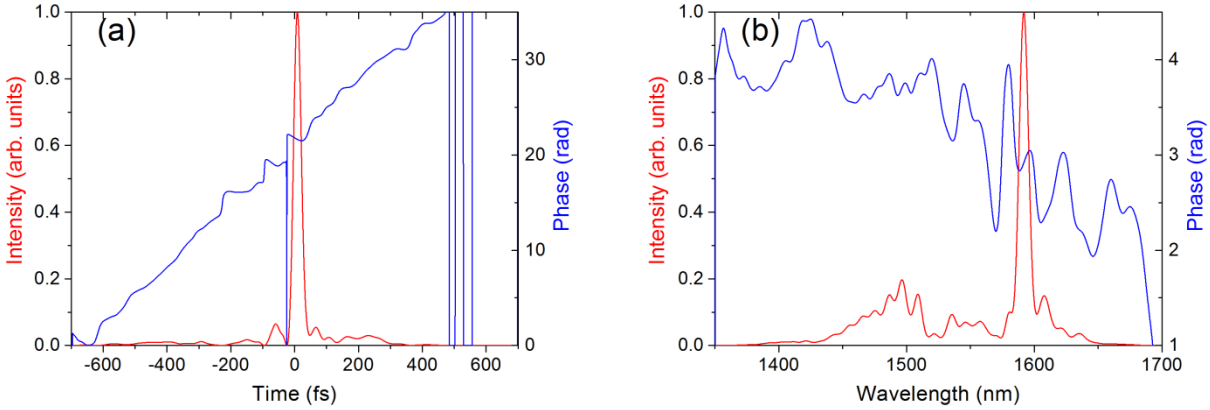


**Fig. 2** (a) retrieved temporal intensity and phase, and (b) retrieved spectral intensity and phase for the 1.56-µm OPCPA seed pulses at the output of the Er-fiber laser module.

**WP1.2: CEP stabilization of the seed laser output at 1.5 µm (Milestone 1)**

Initial questions:

- actual CEP noise and signal-to-noise (S/N) ratio of the CEO beat note,
- spectral phase and available pulse energy after CEP correction.

Actual implementation:

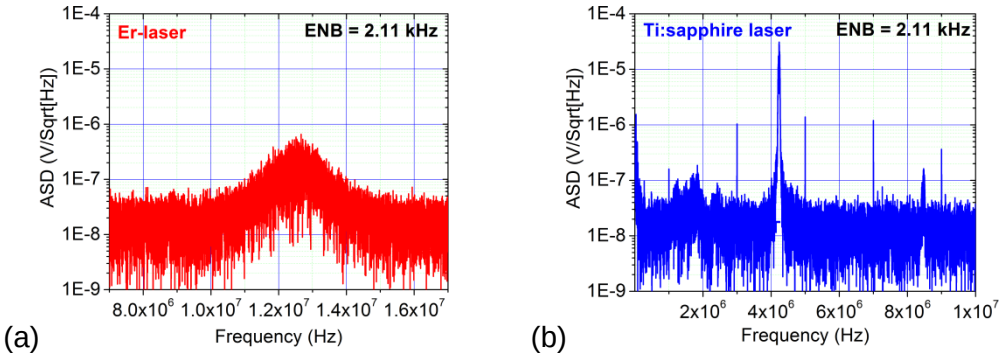


**Fig. 3** RF amplitude spectral density (ASD) measured for (a) the free-running Er-fiber laser and (b) a representative free-running Ti:sapphire laser (EBN: equivalent noise bandwidth). The CEO beat note in panel (b) is at 4.2 MHz.

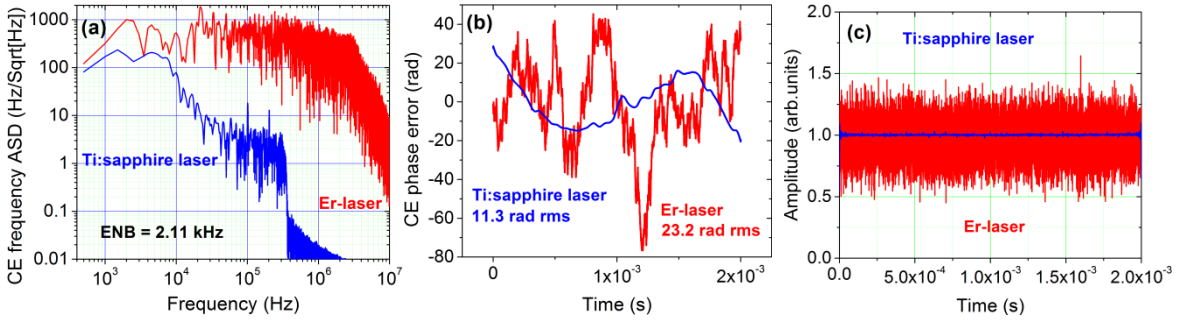


**Fig. 4** Carrier envelope (CE) frequency amplitude spectral density (ASD) (a), carrier envelope (CE) phase jitter (b), and temporal amplitude of the carrier envelope offset beat note measured for the free-running Er-fiber laser (red) and Ti:sapphire laser (blue) from Fig. 3.

The CEP noise was characterized using the commercial f-2f module. The radio frequency (RF) power spectrum provided by the interferometer revealed a very broad carrier envelope offset (CEO) beat note with a very low S/N ratio of only 20 dB, which is 40 dB below that of a standard commercial fs Ti:sapphire oscillator (cf. Fig. 3). The extracted CEP jitter was found to contain a frequency noise spectrum dominated by white noise up to 2-3 MHz, more than two orders of magnitude larger than in the case of a Ti:sapphire laser (cf. Fig. 4 (a)) and well beyond the capabilities of any known CEP stabilization techniques. In addition, an always present CEO drift of ~MHz/min rate was observed. Due to patent issues, the fiber laser manufacturer did not deliver a solution for a slow feed-back loop to stabilize and set the average CEO frequency. Thus, a new method had to be invented before the feed-forward CEP stabilization method could be employed at all [1]. The new method drastically improved the limitations for kHz amplifiers using synthesis of a narrow-band acoustic frequency comb from the measured CEO beat note and the amplifier repetition rate [2]. However, it relied on a narrowband RF bandpass filter in the signal chain of the acousto-optic frequency shifter (AOFS) driver circuit. This, together with the unavoidable acoustic propagation delay in the modulator crystal from the transducer to the interaction volume limited the effective servo bandwidth to a few 100 kHz. To avoid this limitation, an improved version of the acoustic-comb-based feed-forward scheme was developed, enabling an order-of-magnitude increase in servo bandwidth [3,4]. The scheme was implemented for the output of the 80-MHz Er-fiber laser. In order to eliminate the effect of the acoustic delay, we used a 200-m Herriott cell to

delay the optical signal by an amount equal to the acoustic delay in the AOFS. Moreover, the electronics were modified to avoid additional group delays from bandpass filtering (cf. Fig. 5).

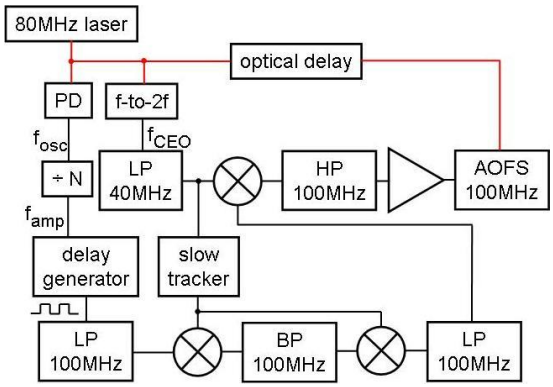


**Fig. 5** Improved acoustic-comb-based feed-forward CEP stabilization scheme. PD: photodiode, ÷N: frequency division, LP: long pass filter: BP: bandpass filter, HP: high pass filter, AOFS: acousto-optic frequency shifter.

The high losses in pulse energy during CEP correction, however, prevented out-of-loop CEP characterization at the convenient 80-MHz repetition frequency. Amplification of the CEP-corrected pulses was needed. This could be achieved only at the repetition rate of the OPCPA (i.e. 100 kHz) after the full pump amplifier chain was implemented. The scheme of out-of-loop CEP characterization is shown in Fig. 6. The out-of-loop f-2f measurements showed a CEP jitter at the > 1-rad level (Fig. 7), which was attributed to CEP noise added by the out-of-loop detection scheme. The source of the added noise was identified as massive amplitude noise of the original CEO beat note (Fig. 4 (c)) used as the seed of the RF driver electronics, which showed a strong correlation with the CEP noise and was unrelated to the actual implementation of the f-2f interferometer [5]. These noise signatures were later identified to originate from the mode-locking mechanism of the Er-laser oscillator. The large amplitude noise rendered the feed-forward method useless, as it resulted in strongly fluctuating laser pulse energy in the CEP-corrected beam, which cannot be used to seed an OPCPA even if the pulses are CEP stabilized. As a different type of mode-locked Er-fiber oscillator with proper parameters is not available from any vendor, active CEP stabilization of the Er-fiber laser was abandoned. Passive CEP stabilization is planned to be implemented in the coming months based on a new, Yb-laser based front-end that is currently being manufactured. This system will moreover provide spectrally much smoother pulses than the current front-end leading to smaller spectral phase modulations during parametric amplification and cleaner recompressed temporal pulse profiles.

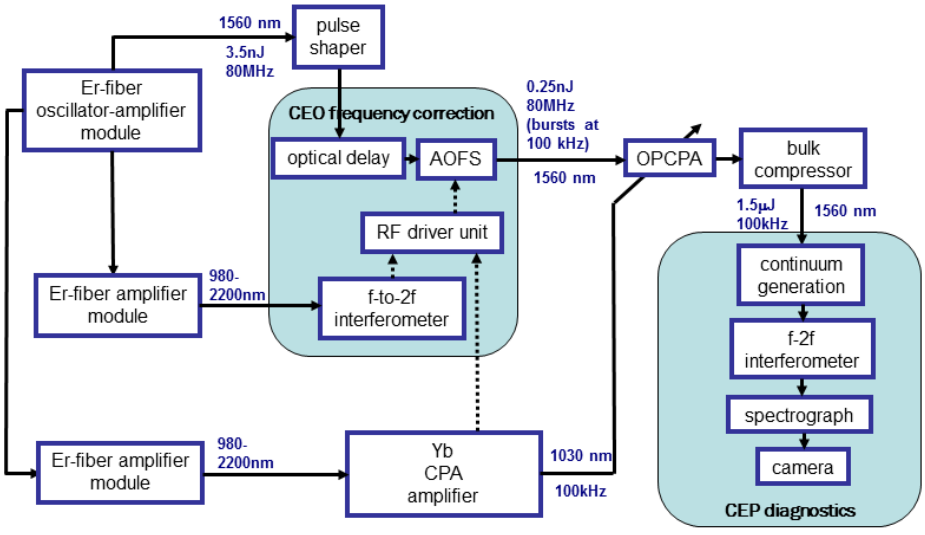


**Fig. 6** Experimental scheme for the out-of-loop characterization of CEP fluctuations.

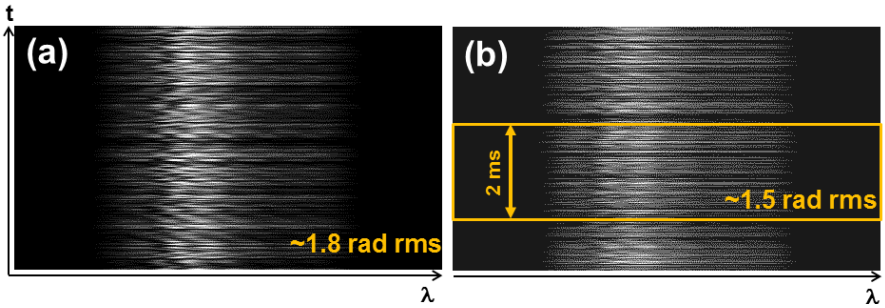


**Fig. 7** Spectral f-2f interference fringes recorded using a home-built interferometer based on a 50-kHz linescan camera, (a) using signal generator as RF seed: 1.8 rad RMS (i.e. random), and (b) using $f_{CEO}$ beatnote as RF seed: segments with nonrandom CEP, 1.5 rad RMS.

In summary, Milestone 1 was not reached during the timeline of the project due to limitations of currently available Er-fiber seed oscillators. However, the valuable experience gathered also stimulated a targeted effort in another MBI lab to develop an alternative bulk laser concept based on Cr:YAG.

**WP1.3: control of spectral phase and amplitude of 1.5-µm seed pulses**

This is a new WP supplanting WP2.2. For details, please see WP2.2.

**WP2: pump booster**

The output of the 1.0-µm supercontinuum branch of the front-end Er-fiber laser system was planned to be amplified in various modules, namely a cw fiber amplifier, a thin-disk regenerative amplifier, and a final Innoslab amplifier. A pulse shaper was intended to be set up to provide temporally super-Gaussian pump pulses to maximize the bandwidth of the amplified signal and idler pulses. As the target pump pulse energy was ≥ 2 mJ, amplification in the chirped pulse concept was necessary with a free-space diffraction grating based compressor module.

**WP2.1: cw-fiber amplifier**

Initial questions:

- minimum input seed average power to ensure amplification at low amplified spontaneous emission (ASE),
- required minimum level of isolation between (i) Er-fiber laser based supercontinuum module and cw-fiber amplifier, and (ii) cw-fiber amplifier and thin disk amplifier,
- cost and delivery time for a home-built versus a commercial solution.

Various issues were raised regarding the originally proposed scheme of the pump CPA chain. One issue was the low expected ASE content, when the fiber amplifier is operated at the full 80 MHz repetition rate at the very low, 2-pJ/nm energy density at 1.0 µm available from the front-end. Also, the cost and delivery time of a home-built solution was not competitive against commercial solutions. Another issue was the difficulty in implementing a thin-disk regenerative amplifier (WP2.3), which would have bridged the gap between the sub-nJ output of the CW-fiber amplifier and the required Innoslab seed of 20 µJ in a 2-nm band centered at 1030 nm. Therefore, we decided to go with a commercial Yb-doped fiber amplifier (YDFA) operating at 100 kHz with an output pulse energy matched to the requirements dictated by the solid state amplifier prior to the Innoslab amplifier (i.e. 20 nJ in a 2-nm band centered at 1030 nm, WP2.3). As the reduction of the repetition rate from 80 MHz to 100 kHz was to be performed by an acousto-optic (AO) pulse picker in the YDFA instead of the Pockels cells in the originally planned regenerative amplifier, the main pulse to adjacent pre- and post-pulse contrast issue had to be handled by using the fastest AO pulse picker in the market. Furthermore, the location of the stretcher (WP2.4.1) had to be moved between the Er-fiber laser based supercontinuum module and the YDFA. A fiber based

stretcher was chosen leading to an average power of 220 µW seeding the YDFA in a 9-nm wide spectral band (WP2.4.1). Keeping the laser pulses in a fiber instead of a free-space solution helped in terms of laser pulse stability and facilitated easy integration with the solid-state pre-amplifier (WP2.3).

**WP2.2: Pulse shaper (Milestone 2)**

Initial questions:

- amount of gain narrowing during parametric amplification with and without pulse shaper,
- thermal stability,
- cost and delivery time.

Actual implementation:

Our numerical simulations showed that spectral gain narrowing, which is primarily due to the high-gain first OPCPA stage would not be a limiting factor in reaching bandwidths supporting the target sub-50-fs pulses, as the high signal-to-pump pulse duration required for high extraction efficiency would only occur in the low-gain, booster stages. Also, our in-house experience showed that there are crucial long-term stability issues with the proposed pulse shaping scheme. In addition, the scheme leads to significant spectral narrowing, which aggravates the implementation of the CPA concept due to the drastically increased chirp rates and distances between the diffraction gratings in the pump stretcher/compressor. Therefore, we decided to avoid the implementation of the scheme and use a spectral and amplitude filter for the OPCPA seed pulses at 1.5 µm instead (new WP1.3). The latter strategy ensures more straightforward chirp compensation at 1.5 µm that can also indirectly be applied to recompress the 3-µm idler wave. The spectral and amplitude filter, manufactured for the 1.33-1.77-µm range, is based on a 640-pixel spatial light modulator in a 4-f stretcher configuration, which provided much higher throughput (i.e. 45%) than the competing solution based on the so-called acousto-optic programmable dispersive filter (i.e. 1%). The shaper came with a chirp compensation algorithm (i.e. multiphoton intrapulse interference phase scan or MIIPS algorithm), which is capable of push-button recompression of the 1.5-µm pulses.

In summary, the modified Milestone 2 was successfully reached.

**WP2.3: 100-kHz thin-disk pre-amplification stage**

Initial questions:

- required minimum pulse energy to ensure low-ASE amplification,
- temporal pulse contrast with respect to main pulse to multi-10-MHz background pulse train,
- required minimum level of isolation between thin-disk pre-amplifier and Innoslab booster amplifier,
- cost and delivery time for a home-built versus a commercial solution.

Actual implementation:

When the minimum pulse energy required to seed the Innoslab amplifier was clarified (i.e. ≥ 20 µJ in a 2-nm band centered at 1030 nm), a suitable pre-amplifier had to be chosen. Initially, we planned to develop in-house a thin-disk regenerative amplifier with a > 100-µJ pulse energy, which would have also allowed preliminary OPCPA tests before the Innoslab amplifier was delivered. Rod-type amplifiers were excluded because of the difficulty to reach sufficiently high pulse energies with our standard design to provide ample headroom to seed the Innoslab. Based on weighted cost, time, and risk considerations, we decided to go with a commercial solution delivered by the manufacturer of the Innoslab amplifier module. This pre-amplifier was to be integrated into the same sealed laser head with the Innoslab module with a fiber port serving as the input port providing an alignment-free solution from the front-end side and facilitating long term alignment stability. The acquiring of the pre-amplifier from

the manufacturer of the Innoslab module also removed one interface between different companies which lowered the risk for the total amplifier line.

**WP2.4: Innoslab booster (Milestone 3)**

The targeted output power (> 200 W) and pulse energy at 100-kHz of this unit was higher than that of any existing system used for pumping high repetition rate OPCPAs. Therefore, a CPA scheme had to be implemented where the compressor had to withstand > 400-W average power with high enough stability and low enough beam distortions for pumping an OPCPA.

**WP2.4.1: setup of stretcher and compressor**

Initial questions:

- required input pulse duration to the Innoslab amplifier and pre-amplifiers to ensure amplification at a sufficiently low B-integral.

Actual implementation:

Instead of the originally proposed home-built, free-space diffraction grating based stretcher and compressor, various changes occurred during implementation. Due to the alterations in WP2.1 and 2.2, a fiber based solution for stretching was more appropriate than a free-space setup. Enclosing the laser pulses in a fiber also avoids detrimental environmental influences and leads to an extremely compact and robust solution. A nonlinearly chirped fiber Bragg grating (CFBG) was chosen, where the higher order dispersion was designed to compensate the significant higher order chirp introduced by the final free-space grating based compressor. Finally, the compressor was also acquired from the manufacturer of the Innoslab amplifier, which led to more straightforward integration and a lower expected risk for the total amplifier chain.

**WP2.4.2: characterization of the Innoslab amplifier module**

Initial questions:

- required minimum pulse energy to ensure low-ASE amplification,
- spatial beam profile, pointing, and power stability.

Actual implementation:

Contrary to the original proposal, testing the Innoslab module at ns seed pulses at < 100-kHz repetition rates was not possible, as the module was not available as a stand-alone unit, but was integrated into a sealed laser head together with the pre-amplifier at a fixed repetition rate. It also turned out that significant beam shaping occurs in the compressor. Therefore, the characterization of the pump beam that is relevant for OPCPA pumping had to be performed on the recompressed beam, i.e. WP2.4.2 and WP2.4.3 had to be combined.

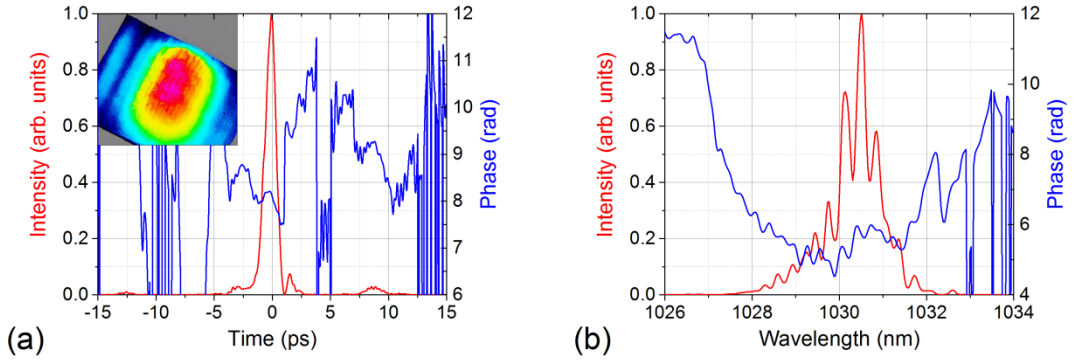


**Fig. 8** (a) temporal intensity and phase and (b) spectral intensity and phase retrieved using SHG-FROG for the recompressed 1.0-µm pump pulses at the 230-W level. The inset in panel (a) shows the recompressed near-field spatial beam profile at full power.

The power stability was found to be excellent: peak-to-peak fluctuations in average power of ± 0.6% in 12 hours. Figure 8 shows the reconstructed temporal and spectral properties of the recompressed pump pulses at full power. The CFBG was identified as the source of the satellite pulse at a delay of ~8 ps from the main pulse. The beam profile at the exit of the compressor is shown in Fig. 8 (a). The side lobes are due to the Innoslab cavity.

Figure 9 (a) shows the excellent $M^2$ beam quality of the recompressed pump beam at the full, 230 W and (b) shows the beam pointing fluctuations measured for the uncompressed beam at 400 W. The short term pointing stability was found to be also excellent. However, there was significant long term beam wander, which required the installation of a piezo-actuated beam stabilization unit to keep the beam direction and location stable for subsequent pumping of the OPCPA.

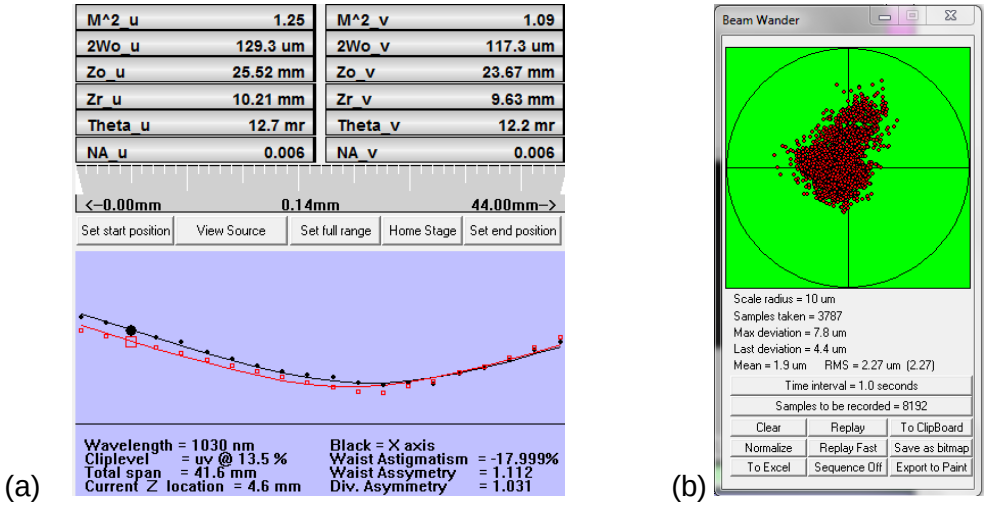


(a) (b)

**Fig. 9** (a) $M^2$ measurement for the recompressed 1.0-µm pump pulses at the 230-W level and (b) beam wander results for the uncompressed 1.0-µm pump pulses at the 400-W level. An f=228 mm lens was used in the beam wander measurement.

**WP2.4.3: set-up and check of the entire CPA system (Milestone 3)**

Initial questions:

- Influence of high average power on the spatial profile and the spatio-temporal behavior.

Actual implementation:

This WP had to be combined with WP2.4.2.

In summary, Milestone 3 was successfully reached.

**WP3: OPCPA**

The original strategy was to seed the OPCPA at 1.5 µm, amplify the signal beam up to the final third stage and extract the 3-µm idler beam only in the last stage. Therefore, a single stretcher based on bulk materials for the 1.5-µm seed and separate compressors for the main 1.5-µm and 3-µm output beams were proposed, respectively. Careful choice and characterization of nonlinear crystals in terms of laser induced damage thresholds was also planned. The target pulse parameters in the two beam lines were:

- 1.5 µm: energy of several 10 µJ, duration at FWHM < 50 fs, CEP stabilized,
- 3 µm: energy of few 10 µJ, duration at FWHM < 50 fs.

**WP3.1: design CPA system at 1.5 µm**

Initial questions:

- Sign of chirp of the 1.5-μm seed beam,
- Pump pulse duration and the optimum ratio of signal-to-pump duration,
- Choice of materials to be used in the stretcher and the two compressors,
- Method to compensate higher order chirp at 1.5 μm.

Actual implementation:

Considering the dispersion properties, bandgap energy, availability of materials and proper anti-reflection (AR) coatings from manufacturers, AR-coated N-SF57 rods were chosen for stretching the 1.5-μm seed. N-SF57 adds positive group delay dispersion (GDD) in the 1.4-1.7-μm range at relatively low third-order dispersion (TOD). During amplification, the generated idler exhibits a reversed sign of GDD relative to the signal, while the TOD does not switch sign and has to be compensated by other means. Therefore, minimization of the total TOD in the beam line was also considered in the design. The compressor for the 1.5-μm beam was based on AR-coated fused silica (FS), which exhibits negative GDD in the 1.4-1.7-μm range. The total length of the FS rods was adjusted to compensate the GDD of the N-SF57 rods. The residual second and higher order chirp was compensated by the 1.5-μm pulse shaper based on the MIIPS algorithm (WP1.3, 2.2). The 1.5-μm pulse shaper was also capable of indirect, manual recompression of the 3-μm pulses thanks to the chirp transfer during parametric amplification. The strategy of recompression was to apply the MIIPS compression algorithm only for the unpumped 1.5-μm OPCPA beamline and then to tune the GDD when the OPCPA was pumped.

**WP3.2: design of compression for 3 μm**

Initial questions:

- Sign of chirp of the generated idler wave,
- Choice of materials to be used in the compressor,
- Method to compensate higher order chirp at 3 μm.

Actual implementation:

The design in WP3.2 had direct influence on the design of the compressor of the 3-μm beam line. AR-coated silicon (Si) was chosen as the bulk compressor due to its high bandgap energy, positive GDD near 3 μm and wide availability. Its thickness was fine-tuned using AR-coated Si wedges to accurately compensate the GDD acquired in the 3-μm idler beam during parametric amplification.

**WP3.3: selection and characterization of nonlinear crystals**

Initial questions:

- Choice of nonlinear crystals and OPCPA geometry for different stages,
- Laser induced damage threshold of nonlinear crystals at the relevant laser parameters.

Actual implementation:

Systematic, R-on-1 laser-induced damage threshold measurements were performed on a wide range of $LiNbO_3$ (LN) and rubidium-doped $KTiOPO_4$ (RKTP) crystals at the relevant 1.03-μm wavelength. The LN samples included uncoated and anti-reflection coated, blank and periodically poled (PP) MgO-doped congruent crystals and were measured at repetition rates between 10-1000 kHz, pulse durations of 0.33 and 1 ps, and temperatures between 20 and 170 $^{o}$C [6]. The measurements on RKTP were performed on blank, uncoated samples at pulse durations of 0.33 and 0.93 ps, at a repetition rate of 100 kHz, including temperature dependence [7]. Based on the damage threshold measurements and available sample thickness, PPLN was chosen as the amplifying material for the first OPCPA stage and blank $KTiOAsO_4$ for the two consecutive stages.

**WP3.4: final test and characterization (Milestone 4)**

Originally, a three-stage OPCPA was planned, pumped with the full power of the pump laser.

Actual implementation:

A two-stage OPCPA front-end was implemented and characterized [8], where 25% of the full pump power was utilized. Despite being pumped by only a small fraction of the full power, this front-end was already providing world record parameters at 1.55 µm exceeding those in Ref. [9] and satisfying the project goals except for the CEP-stability. Therefore, we started the application experiments prior to implementing the third OPCPA stage. The current scheme is shown in Fig. 10. Stage 1 is based on a 2-mm-long, AR-coated, 5%-MgO-doped, fanout PPLN crystal used in collinear geometry. Seeded by 1-nJ stretched 1.56-µm pulses and pumped by 2.5 W, the first stage provides a gain of 1400 and an output signal pulse energy of 1.4 µJ. The idler beam at 3.1 µm generated in the first stage is filtered out by dichroic optics. The full optics chain supports a spectral bandwidth for 34-fs pulses. There is negligible spectral narrowing in the first stage with a Fourier limit of 35 fs at 1.55 µm. The signal pulses are then further stretched by an additional AR-coated N-SF57 block to reduce the pump to signal pulse duration ratio and therefore increase the conversion efficiency in the second OPCPA stage. The second OPCPA stage is a 4-mm-thick, AR-coated KTA crystal used in noncollinear, type-II arrangement and pumped by an average power of 57 W. In contrast to [8], the pump power was increased and the conversion efficiency was reduced to ~16% in the second stage to keep the Strehl ratio high for application experiments. The output pulse energy after the KTA crystal is typically 90±3 µJ depending on alignment. The amplified signal pulses are upcollimated and sent through 31-cm of AR-coated FS with 96% throughput.

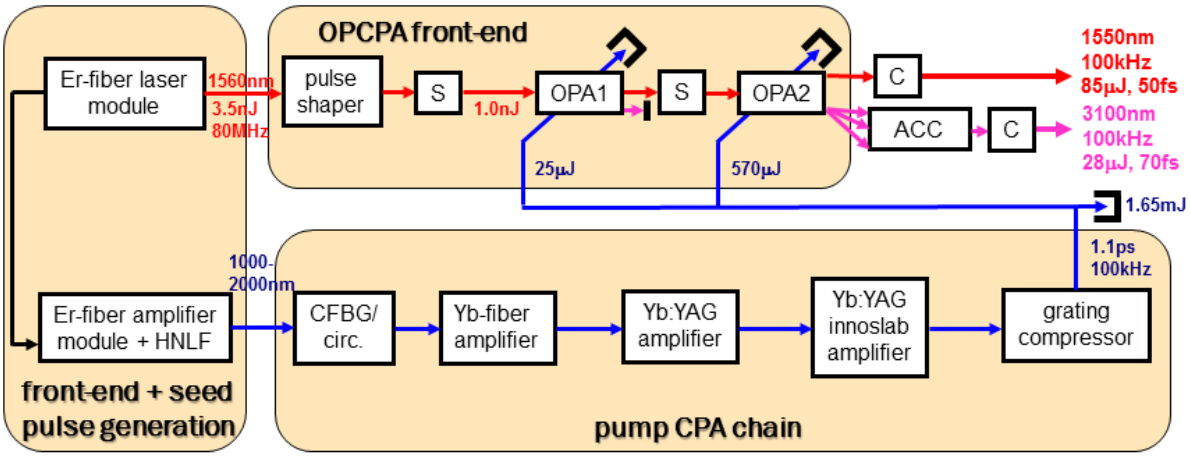


**Fig. 10** Current scheme of the OPCPA. S: bulk stretcher, C: bulk compressor, ACC: angular chirp compensation.

Using the strategy described in WP3.1, successful recompression was achieved approaching the ~45-fs transform limited duration at the 90-µJ pulse energy level. A typical SHG-FROG trace and retrieval results are shown in Fig. 11 and 12, respectively. The recompressed pulse duration is typically in the 47-52-fs range. The minor variation from day to day is due to slightly different alignment conditions. The recompressed pulses are not clean, but contain a long pedestal. The origin of this pedestal is attributed mainly to parasitic frequency conversion effects in the PPLN-based first OPCPA stage and the strongly modulated spectrum. Removal of the pedestal using the pulse shaper in the 1.5-µm beam line was not successful. The difficulty is due to the fact that the spectral phase distortions are not polynomial and that there is a complicated interplay between the phase mask loaded onto the pulse shaper and the spectral phase and even pulse energy after the pulses are amplified.

The beam profile of the 90-µJ signal pulses is excellent as demonstrated by the inset in Fig. 12 (a). As a comparison, Ref. [9] reported a record high average power system, where the

1.54-µm beam line parameters were 75 µJ and 98 fs at a repetition rate of 100 kHz. The average power stability of the recompressed signal beam in our case is 0.5% RMS for a duration of 1 hour. The excellent power stability is due to an active timing jitter compensation setup based on a high speed piezo based, servo controlled translation stage, which turned out to be crucial for keeping the OPCPA output stable. As expected, the timing jitter was dominated by the amplifiers and not the Er-fiber laser front-end (WP1.1).

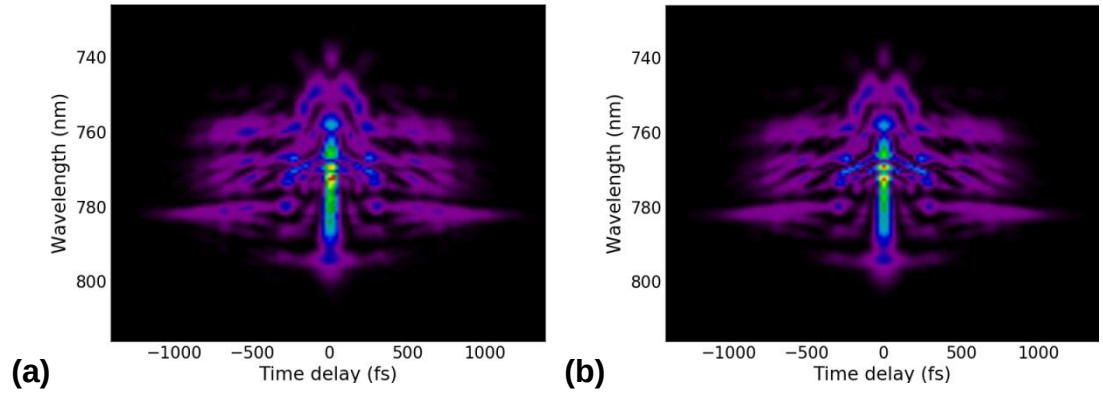


**Fig. 11** (a) measured SHG-FROG trace, (b) reconstructed SHG-FROG trace for the recompressed 1.5-µm signal pulses at the 90-µJ level.

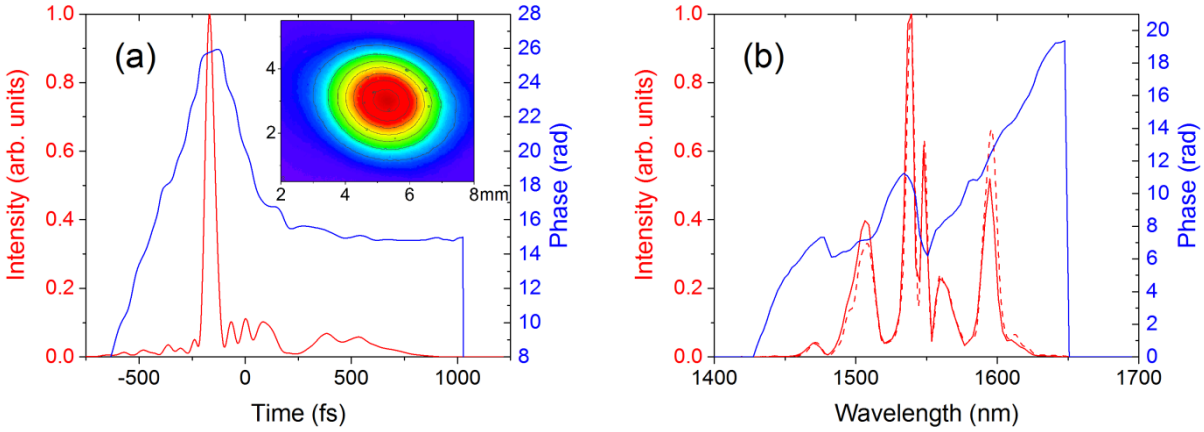


**Fig. 12** (a) retrieved temporal intensity and phase, (b) retrieved spectral intensity and phase for the recompressed 1.5-µm signal pulses at the 90-µJ level (corresponding to the trace shown in Fig. 11). The retrieved pulse duration (FWHM) is 52 fs. The inset in panel (a) shows the Gaussian spatial beam profile with $w_{1/e}^2$(horizontal) = 2.1 mm and $w_{1/e}^2$(vertical) = 1.8 mm. The dashed line in panel (b) shows the measured spectrum.

Due to the noncollinear geometry of the second OPCPA stage, the generated 3.1-µm idler beam is angularly dispersed and propagates in a direction different from the direction of the signal beam. The measured pulse energy at 3.1 µm after the KTA crystal is 45 µJ (i.e. 50% of the signal pulse energy). The pulse energy and spectral bandwidth of the idler output of the second OPCPA are very competitive when compared to existing 3-µm state-of-the-art high repetition rate systems [11-13]. However, due to the strong angular dispersion in noncollinear OPCPAs, such beams are typically considered useless and are discarded.

Despite the strong angular dispersion, we successfully implemented an angular chirp compensation scheme with a throughput of 66%. Figure 13 shows the beam profile of the angularly corrected idler beam measured along a 1-m path after a telescope meters behind the KTA crystal. The small residual astigmatism and spatial chirp can be improved by appropriate optics in a straightforward way, when needed. The large, 80-µm pixel size of our mid-infrared camera prevented an $M^2$ measurement so far. After angular dispersion had been corrected, recompression of the idler beam became possible.

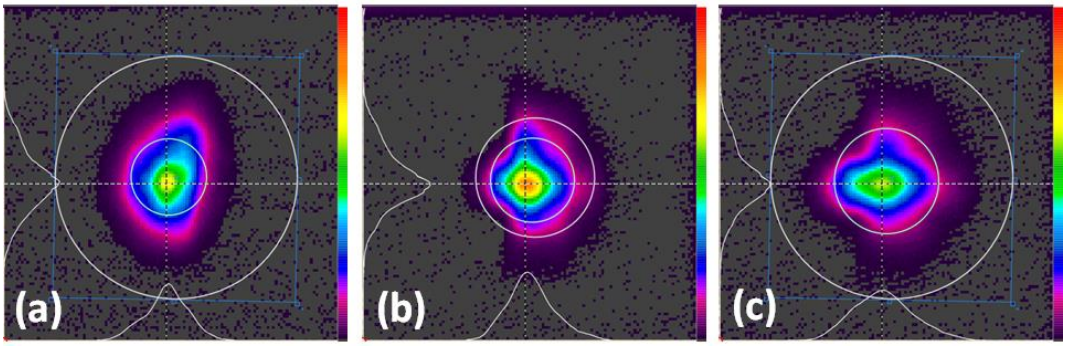


**Fig. 13** Beam profiles of the angular chirp corrected 3.1-µm beam measured 7 cm (a), 69 cm (b), and 98 cm (c) behind a down-collimating telescope, which was 2 m behind the KTA crystal. The chip size was 12.8x12.8 mm and the ISO 4σ diameter of the beam in panel (b) is 2.9 and 3.9 mm in the horizontal and vertical plane, respectively.

Based on the strategy described in WP3.2, successful recompression was achieved to near the ~65-fs transform limited duration at a pulse energy of up to 30 µJ. A typical SHG-FROG trace and retrieval results are shown in Fig. 14 and 15, respectively. The recompressed pulse duration is typically in the 69-72-fs range. Even though the pulse duration at FWHM is only 70 fs, there is a significant pedestal similar to the case of the 1.5-µm beam line. As a comparison, the pulse duration and energy of existing state-of-the-art sources reported in Ref. [11], [12], and [13] were (i) 44 fs and 22 µJ at 50 kHz, (ii) 55 fs and 20 µJ at 160 kHz, and (iii) 72 fs and 10 µJ at 125 kHz, respectively.

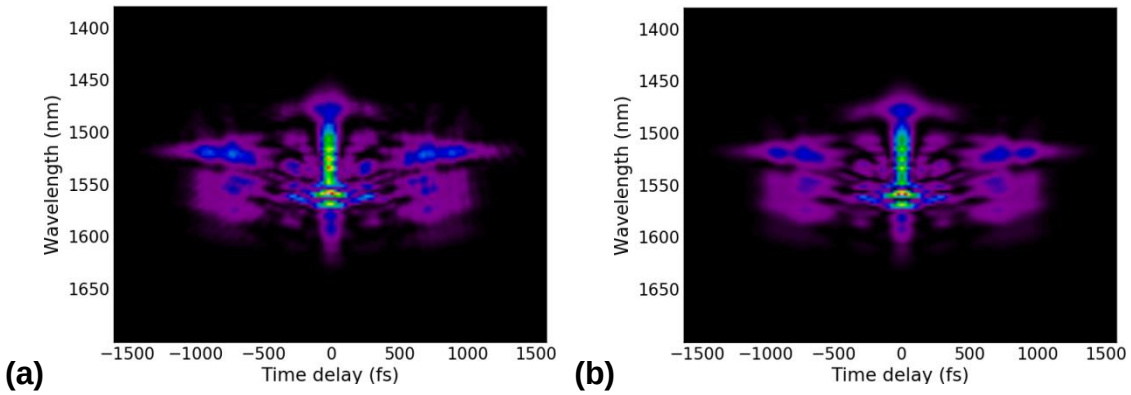


**Fig. 14** (a) measured SHG-FROG trace, (b) retrieved SHG-FROG trace for the recompressed 3.1-µm pulses at the 30-µJ level.

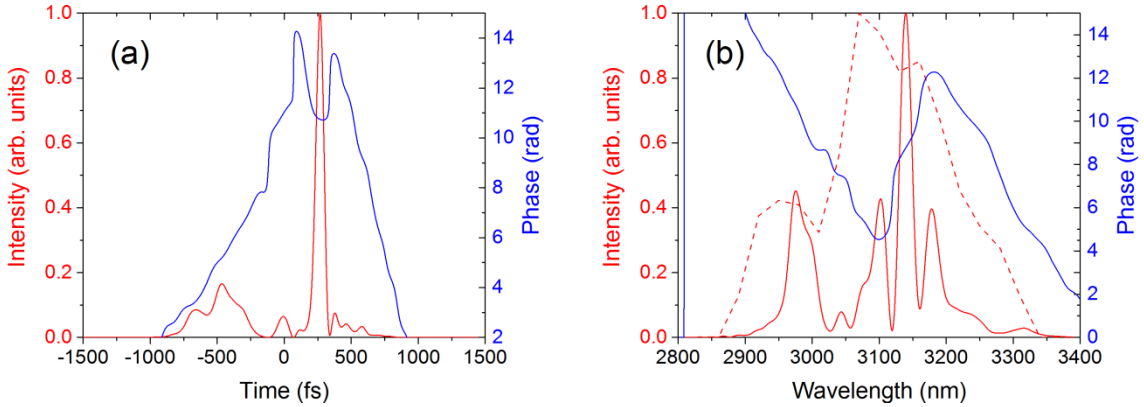


**Fig. 15** (a) retrieved temporal intensity and phase, (b) retrieved spectral intensity and phase for the recompressed 3.1-µm pulses at the 30-µJ level (corresponding to the trace shown in Fig. 14 and measured simultaneously to the 1.5-µm trace shown in Fig. 11). The retrieved pulse duration at FWHM is 70 fs. The dashed line in panel (b) shows the measured spectrum.

The power stability of the recompressed idler beam is excellent thanks to the active timing jitter compensation setup (cf. Fig. 16). In the measured 1-hour time window, this power stability is equivalent to the stability of the system reported in [12] and superior to that reported in [13].

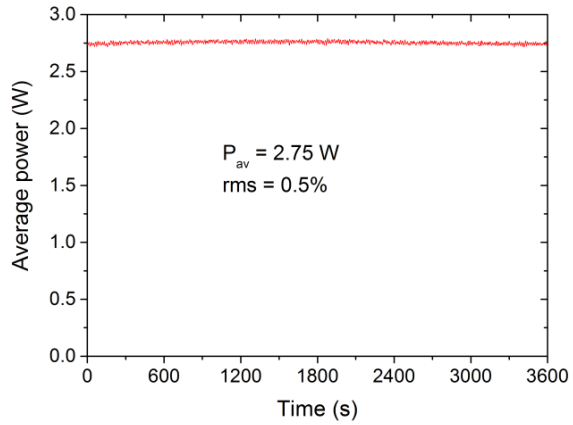


**Fig. 16** Average power stability of the recompressed idler beam.

As a demonstration of the utility of the recompressed idler beam, a fraction of the beam was focused into a sapphire window and a multi-octave supercontinuum was generated, which extended from 450 nm to the midwave-infrared. The blue edge of the supercontinuum was recorded by a CCD spectrometer, see Fig. 17. Similar continua produced by existing 3-μm OPCPA systems were reported in [14,15].

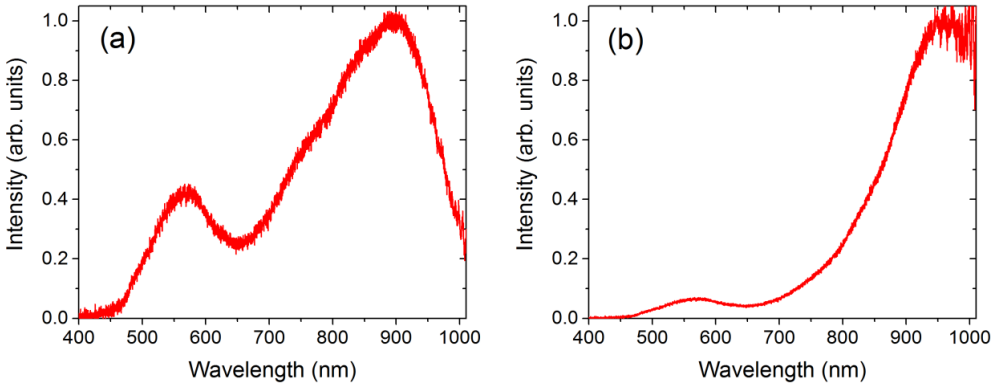


**Fig. 17** Blue edge of the spectrum of a multi-octave supercontinuum generated in a sapphire plate by recompressed 3.1-μm pulses: (a) raw, (b) corrected for wavelength dependent quantum efficiency of the CCD.

In summary, despite of implementing only a two-stage OPCPA front-end pumped by 25% of the total pump power, the target pulse energy values were reached both at 1.5 and 3 μm. Regarding pulse duration, the target was reached only at 1.5 μm. In the next few months, the third OPCPA stage will be added to the system with a tentative scheme and parameters shown in Fig. 18, which will dramatically widen the range of possible spectroscopic applications.

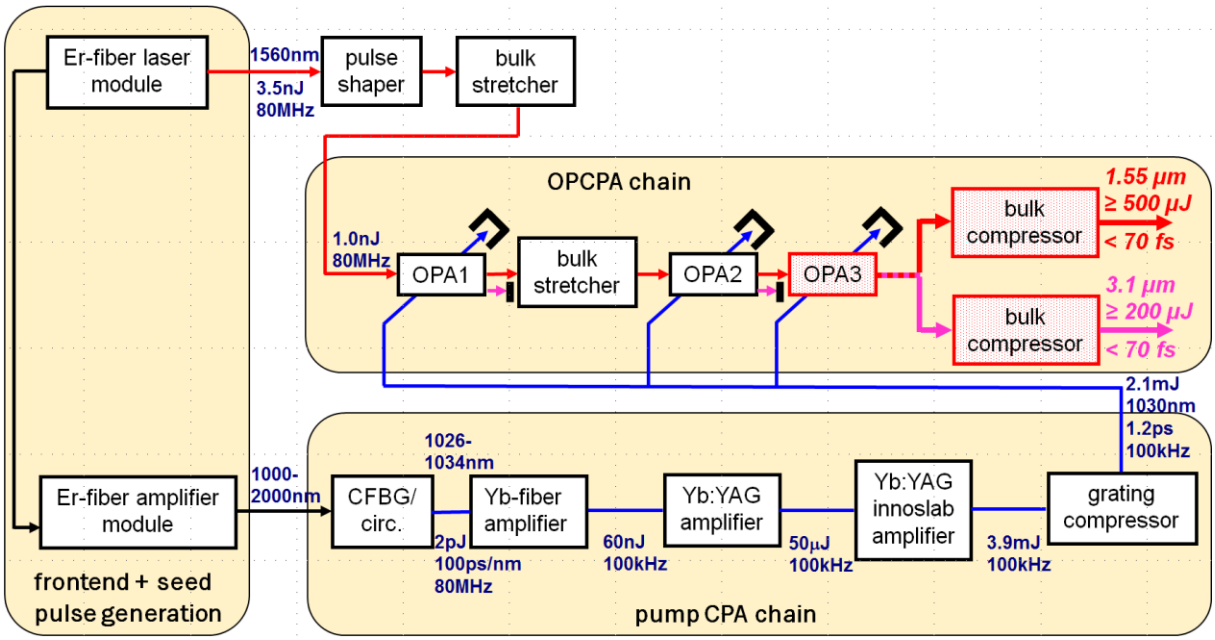


**Fig. 18** Future scheme of the final OPCPA system.

**WP4: Application test**

**WP4.1: characterization of OPCPA stage 1 and 2**

Initial questions:

- CEP jitter after the first two OPCPA stages provided that the seed at 1.5 µm is successfully CEP stabilized.

Actual implementation:

As CEP stability of the 1.5-µm was not achieved (WP1.2) and a thin-disk pre-amplifier was not implemented (WP2.3), this WP was not accomplished.

**WP4.2: electron dynamics induced in noble gas dimers and trimers**

The experiments in the original proposal on noble gas dimers and trimers required CEP stabilization of the system, which was so far not achieved, and which is expected to be available once the front-end has been exchanged (see WP1.2). Therefore, a series of experiments on Coulomb explosion of $CO_2$, water, and acetone were performed to validate the performance of the OPCPA system under realistic experimental conditions. For details, please see the section on molecular fragmentation dynamics below.

**WP4.3: time resolved electron holography (Milestone 5)**

In parallel to the development of the pump amplifier and the OPCPA, first experiments on time-resolved electron holography were carried out using an available kHz Ti:Sapphire laser. Given the lower repetition rate of this laser (compared to the OPCPA developed in the project), these experiments did not measure electron and ion signals in coincidence, but were limited to electron-only measurements using a velocity map imaging detector.

In a first series of experiments using $CF_3I$ molecules, photoelectron momentum maps were compared for intense field ionization of impulsively aligned and anti-aligned molecules at 800-nm and 1.3-µm laser wavelengths. Pronounced Laser-Induced Electron Diffraction (LIED) effects were observed in the high-energy re-collision plateau. Remarkably, a comparison of the experimental results with ab-initio calculations based on time-dependent density functional theory (TDDFT) revealed that the observed diffraction pattern is dominated by recollision from electrons originating from ionization of the HOMO-1 orbital.

In a second series of experiments, $I_2$ molecules were optically exited to the electronic A- and B-states, and photoelectron momentum maps were recorded at several time delays, clearly revealing the time-evolution of the internuclear distance.

Together, these two experiments provide a set of benchmarks that will be investigated further in the future by means of electron-ion coincidence experiments with the newly developed OPCPA.

**Fragmentation dynamics of simple molecules by strong 1.55-µm fields**

Fragmentation dynamics of carbon dioxide ($CO_2$), water ($H_2O$), and acetone ($C_3H_6O$) were measured using a recently developed ion-ion coincidence momentum map imaging spectrometer based on a so-called Timepix detector. As an example, results obtained for acetone using the 1.5-µm source are shown below. The data analysis of these results is currently ongoing. Figure 19 shows time-of-flight spectra of ions following strong field ionization of acetone at different laser intensities. At the weakest laser intensity, besides the parent ion, only $H^+$, $CH_3^+$ and $COCH_3^+$ ion fragments are dominant (cf. red line in the Fig. 19). These fragments can be attributed to the pathways summarized in the first column of Table 1. In contrast, at higher intensities, more complex fragmentation processes occur resulting in many more fragment ions including highly charged fragment ions such as $C_3^+$, $O_3^+$, $C_2^+$, $O_2^+$ (cf. blue line in Fig. 19). The photoion-photoion coincidence image shown Fig. 20(a) suggests that several ion-pairs display correlated times-of-flight (TOFs). The Coulomb explosion channel ($CH_3^+$ + $COCH_3^+$) predominates in the dissociative process of acetone, in agreement with the $COCH_3^+$ ion image shown in Fig. 20(b). The outer ring of the distribution is assigned to the Coulomb explosion channel (i.e. $CH_3^+$ + $COCH_3^+$), while the inner distribution may be due to direct dissociation of the singly-charged parent molecular ion. The image in Fig. 20(b) suggests that the fragment ions $CH_3^+$ and $COCH_3^+$ are emitted along the laser polarization direction with angular distribution with constant width with respect to the laser polarization. This may indicate that prior to Coulomb explosion, the two C-C bonds are bent to form a linear C-C-C structure. Similar nuclear dynamics before Coulomb explosion were also observed in the dissociative double ionization of $H_2O$. All possible pathways including the formation of doubly charged ions (with and without hydrogen eliminations) are listed in the second and third column of Table 1.

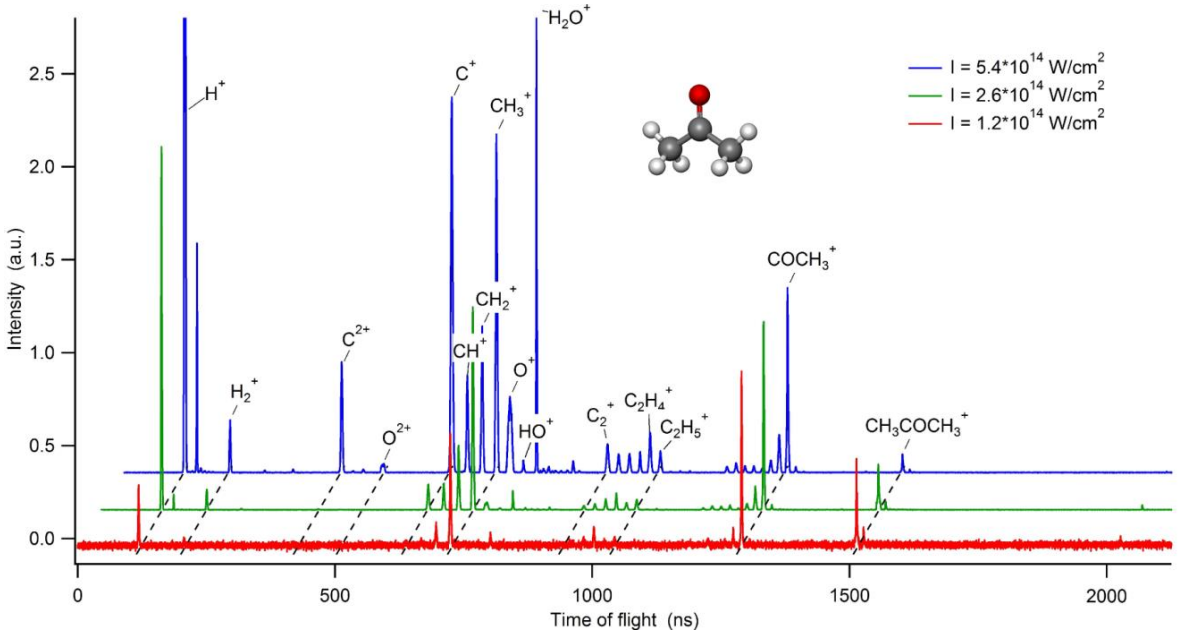


**Fig. 19** Measured time-of-flight spectra of ions following fragmentation of acetone. All spectral peaks are normalized to the peak height of the $COCH_3^+$ ion in order to show the relative intensity variation of other fragments at different laser intensities.

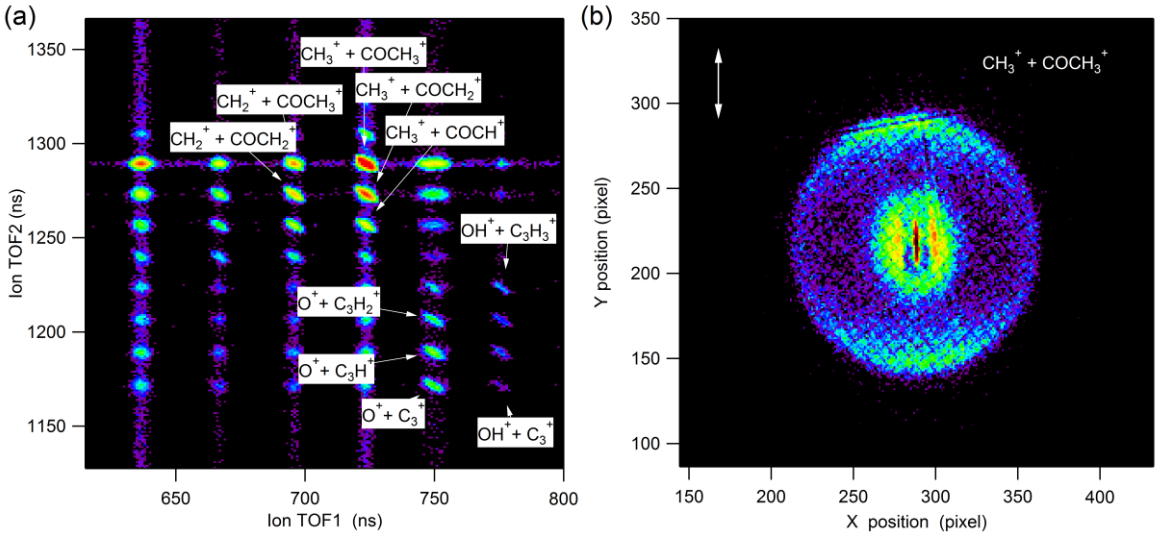


**Fig. 20** (a) Photoion-photoion coincidence distribution. (b) Measured image of $COCH_3^+$ from the channel ($CH_3^+$ + $COCH_3^+$). The laser polarization direction is indicated as a double- arrow line. The laser intensity was 5.4 × $10^{14}$ W/$cm^2$ at a pulse duration of 50 fs.

**Table 1** Major dissociative pathways after acetone was ionized by the 1.55-μm laser field.

| Singlet charged<br>$CH_3COCH_3 \rightarrow CH_3COCH_3^+$ | Doubly charged<br>$CH_3COCH_3 \rightarrow CH_3COCH_3^{2+}$ | Doubly charged with Hydrogen elimination |
|---|---|---|
| $\rightarrow CH_3^+ + COCH_3$<br>$\rightarrow CH_3 + COCH_3^+$<br>$\rightarrow H^+ + CH_2COCH_3$ | $\rightarrow$ **$CH_3^+ + COCH_3^+$** (dominant)<br>$\rightarrow$ **$CO^+ + CH_3CH_3^+$** (slight, methyl migration) | $CH_3COCH_2^{2+} \rightarrow CH_3^+ + COCH_2^+$<br>$CH_3COCH^{2+} \rightarrow CH_3^+ + COCH^+$<br>$CH_3COCH^{2+} \rightarrow CH_3^+ + COC^+$ |
| | | $CH_2COCH_3^{2+} \rightarrow CH_2^+ + COCH_3^+$<br>$CHCOCH_3^{2+} \rightarrow CH^+ + COCH_3^+$ |
| | | $COC_2H_3^{2+} \rightarrow O^+ + C_3H_3^+$<br>$COC_2H_2^{2+} \rightarrow O^+ + C_3H_2^+$<br>$COC_2H^{2+} \rightarrow O^+ + C_3H^+$<br>$COC_2^{2+} \rightarrow O^+ + C_3^+$ |
| | | **$COHC_2H_3^{2+} \rightarrow OH^+ + C_3H_3^+$**<br>**$COHC_2H_2^{2+} \rightarrow OH^+ + C_3H_2^+$**<br>**$COHC_2H^{2+} \rightarrow OH^+ + C_3H^+$**<br>**$COHC_2^{2+} \rightarrow OH^+ + C_3^+$**<br>(hydrogen migration) |

## References

[1] B. Borchers, M. Mero, and G. Steinmeyer, "Acoustic frequency combs for unconditionally stable long-term carrier-envelope phase stabilization," Conference on Lasers and Electro-Optics 2013, OSA Technical Digest (online) (Optical Society of America, 2013), CTh4M.2.

[2] B. Borchers, F. Lücking, and G. Steinmeyer, “Acoustic frequency combs for carrier-envelope phase stabilization,” Opt. Lett. **39**, 544 (2014).
[3] M. Mero, N. Raabe, and G. Steinmeyer, "Long-term, real-time correction of carrier-envelope phase fluctuations," 2015 European Conference on Lasers and Electro-Optics - European Quantum Electronics Conference (Optical Society of America, 2015), CF_4_3.
[4] German patent registration 10 2015 200 668.9 “Verfahren und Vorrichtung zum Erzeugen eines Steuersignals für ein akusto-optisches Bauelement zur Carrier-Envelope-Phasenstabilisierung” by F. Bach, M. Mero, and G. Steinmeyer.
[5] N. Raabe, M. Mero, Y. Song, W. Haensel, R. Holzwarth, A. Sell, A. Zach, and G. Steinmeyer, "Detecting determinism in laser noise: a novel diagnostic approach for ultrafast lasers," Conference on Lasers and Electro-Optics 2016, OSA Technical Digest (Optical Society of America, 2016), SM3I.5.
[6] F. Bach, M. Mero, M.-H.-Chou, F. Noack, and V. Petrov, "High-average-power, picosecond laser induced damage behavior of blank lithium niobate crystals at 1030 nm," Advanced Solid State Lasers 2015, OSA Technical Digest (online) (Optical Society of America, 2015), ATu2A.4.
[7] F. Bach, M. Mero, V. Pasiskevicius, A. Zukauskas, and V. Petrov, "High repetition rate, femtosecond and picosecond laser induced damage thresholds of Rb:$KTiOPO_4$ at 1.03 μm," Lasers Congress 2016 (ASSL, LSC, LAC) OSA Technical Digest (online) (Optical Society of America, 2016), JTu2A.31.
[8] M. Mero, F. Noack, F. Bach, V. Petrov, and M. J. J. Vrakking, “High-average-power, 50-fs parametric amplifier front-end at 1.55 μm,” Opt. Express **23**, 33157 (2015).
[9] Y. Shamir, J. Rothhardt, S. Hädrich, S. Demmler, M. Tschernajew, J. Limpert, and A. Tünnermann, “Short-IR GW peak power OPCPA system with record average power at 100 kHz for high field physics,” Advanced Solid State Lasers 2015, OSA Technical Digest (online) (Optical Society of America, 2015), AW3A.3.
[10] Y. Shamir, J. Rothhardt, S. Hädrich, S. Demmler, M. Tshernajew, J. Limpert, and A. Tünnermann, “High-average-power 2 μm few-cycle optical parametric chirped pulse amplifier at 100 kHz repetition rate,” Opt. Lett. **40**, 5546 (2015).
[11] B. W. Mayer, C. R. Phillips, L. Gallmann, and U. Keller, "Mid-infrared pulse generation via achromatic quasi-phase-matched OPCPA," Opt. Express **22**, 20798 (2014).
[12] M. Baudisch, B. Wolter, M. Pullen, M. Hemmer, and J. Biegert, "High power multi-color OPCPA source with simultaneous femtosecond deep-UV to mid-IR outputs," Opt. Lett. **41**, 3583 (2016).
[13] P. Rigaud, A. V. de Walle, M. Hanna, N. Forget, F. Guichard, Y. Zaouter, K. Guesmi, F. Druon, and P. Georges, "Supercontinuum-seeded few-cycle mid-infrared OPCPA system," Opt. Express **24**, 26494 (2016).
[14] F. Silva, D.R. Austin, A. Thai, M. Baudisch, M. Hemmer, D. Faccio, A. Couairon, and J. Biegert, "Multi-octave supercontinuum generation from mid-infrared filamentation in a bulk crystal," Nat. Commun. **3**, 807 (2012).
[15] A. Choudhuri, A. Ruehl, I. Leon, N. DiPalo, I. Hartl, R.J. Dwayne Miller, and J. Biegert, "Multi-octave supercontinuum generation driven by few-cycle mid-IR pulses in YAG, ZnSe and sapphire," Conference on Lasers and Electro-Optics 2016, OSA Technical Digest (online) (Optical Society of America, 2016), FF1M.2.
[16] X.-P. Tang, S.-F. Wang, M. E. Elshakre, Li-R. Gao, Y.-L. Wang, H.-F. Wang, and F.-A. Kong, “The field-assisted stepwise dissociation of acetone in an intense femtosecond laser field,” J. Phys. Chem. A **107**, 13 (2003).
[17] R. J. Levis, G. M. Menkir, and H. Rabitz, “Selective bond dissociation and rearrangement with optimally tailored, strong-field laser pulses,” Science **292**, 709 (2001).
[18] P. Maierhofer, M. Bainschab, B. Thaler, P. Heim, W. E. Ernst, and M. Koch, “Disentangling multichannel photodissociation dynamics in acetone by time-resolved photoelectron–photoion coincidence spectroscopy,” J. Phys. Chem. A **120**, 6418 (2016).

**Statement about economical viability**

The project resulted in the filing of a patent [4], where commercial exploitation is expected.

**Cooperation partners**

- University of Konstanz: components used for CEP noise measurement,
- HC Photonics: nonlinear crystal samples for laser induced damage studies.

**Qualification work resulting from the project**

- Florian Bach, Ph.D. defense to take place in Spring 2017.

**Presentation of measures to ensure security and availability of research data**

http://intern.mbi-berlin.de/en/organization/good_scientific_practice/rules.html

**List of publications**

First 8 papers listed under References.

**List of press releases**

Not applicable.